Stanford Exploration Project, Report 103, April 27, 2000, pages 1–48

Wave-equation migration velocity analysis: Episode II

Paul Sava and Biondo Biondi[1]

ABSTRACT

We elaborate the main points of the wave-equation migration velocity analysis method introduced in a previous report. We analyze its strengths and limitations, and illustrate them using a synthetic example. The inversion results confirm our original expectations, especially with regard to stability and robustness. The main difficulty in recovering a complete velocity perturbation is related to the Born approximation, which limits the amount of residual migration improvement on the seismic images at any one given step.

INTRODUCTION

Migration and velocity analysis are intertwined components of seismic imaging. Depth migration cannot be done without knowledge about the velocity model, nor can velocity analysis be done without reasonably accurate seismic images. Furthermore, because migration and migration velocity analysis are complementary objects, it makes intuitive sense to require that both are based on the same physics of wave propagation, namely either on the band-limited wave-equation or its high-frequency asymptotic.

Our previous publication (Biondi and Sava, 1999) introduced the concept of wave-equation migration velocity analysis (WEMVA) as the natural counterpart of wave-equation migration. The objective of our method is to exploit in the velocity analysis context the main strengths of processing based on the wave-equation: accuracy, multipathing, and stability.

In addition to its wave-equation nature, another important concept exploited by our method is that of velocity analysis by image enhancement, in contrast to other methods that also use wave-equation techniques but aim at fitting the recorded data. Our method operates by recursively and simultaneously improving both the migrated image and the velocity model. The advantage of doing so is that the users have an opportunity to quality control the results at every step.

In this paper, we briefly review the theory of WEMVA and show a complete synthetic example in which we start with simulated data, create an image with an approximate velocity model, and then improve both the velocity and the image using WEMVA.

[1]**email:** paul@sep.stanford.edu, biondo@sep.stanford.edu

The WEMVA puzzle relies on several key ingredients, among which some of the most important are image enhancement by residual migration, image quality control in the angle-domain and inversion that uses model constraints. All these are briefly discussed in this paper and are demonstrated with our example.

THEORY

In wave-equation migration, data recorded at the surface are recursively downward continued in depth to generate the wavefield at every depth level (Figure 1). Once the complete wavefield is generated, we can apply an imaging condition to obtain the image at every depth level. In practice, however, downward continuation and imaging are merged into one step, so that we do not need to store the complete downward continued wavefield for all frequencies.

The imaging process described in the preceding paragraph requires that we make an assumption about the slowness model. We label this slowness the background model; therefore, the wavefield and image generated using this model are also naturally labeled as the background wavefield and image.

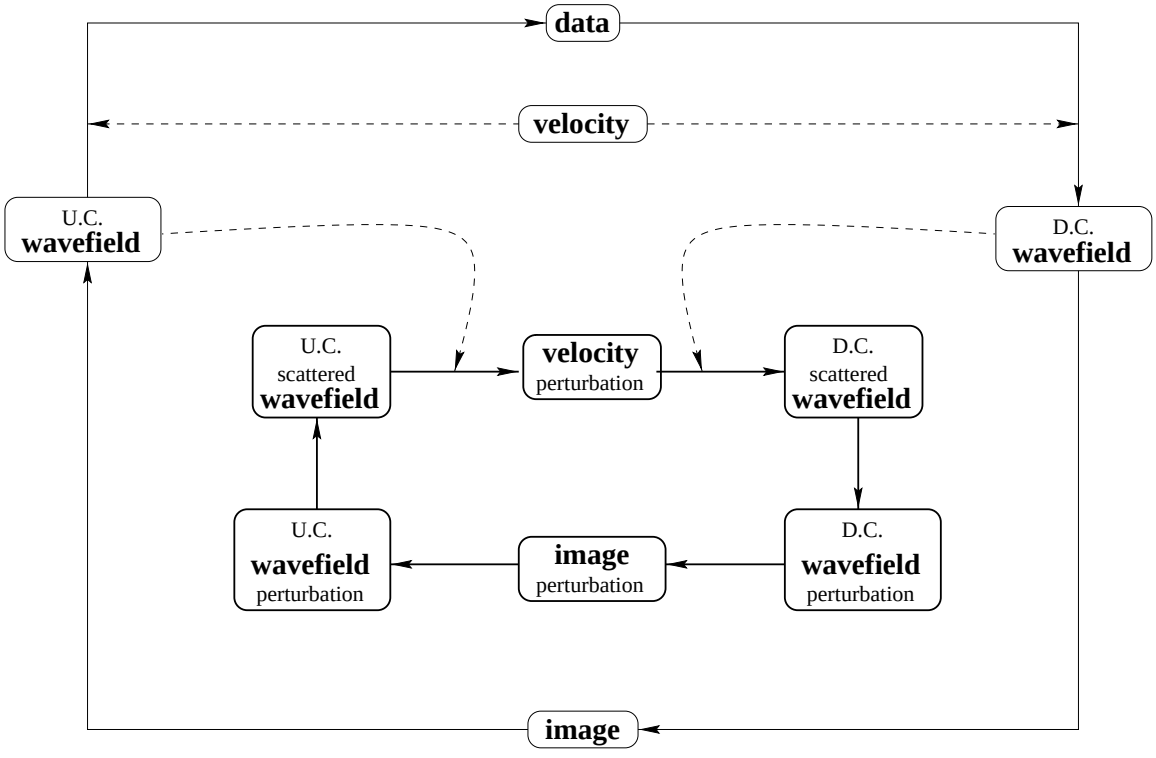

Figure 1: The chart of wave-equation migration velocity analysis technique. D.C. is a label for objects involved in the downward continuation branch, while U.C. is a label for the similar objects of the upward-continuation branch. paul3-core [NR]

Wave-equation modeling, the adjoint of migration, proceeds by upward-continuing the data from the highest depth and by adding contributions at every depth level. Eventually, we

reach the surface and reconstruct the wavefield at the surface, which is equivalent, but not identical, to the recorded data.

A perturbation in the slowness model, excited by the background wavefield, generates a scattered wavefield. Like the background wavefield, this is downward continued, creating a wavefield perturbation, and is imaged, creating an image perturbation. In practice, we can either compute the background wavefield at the same time we compute the scattered wavefield, or we can compute and store it before, one frequency at a time.

As for the background, the adjoint process takes us from the image perturbation to an upward-continued wavefield from which we can derive at every depth level a scattered wavefield and, furthermore, a slowness perturbation.

This is the core theoretical result of the wave-equation migration velocity analysis technique: we can relate a perturbation in the slowness model to a perturbation in the migrated image. This enables us to improve the slowness model at the same time we improve the migrated image. This observation formally materializes a well-known concept: migration and velocity analysis are fundamentally related and inseparable from each other (Gray, 1998). This concept is not particular to our method, although the power of WEMVA lies in that it formally eliminates the distinction between velocity analysis and migration and aims at one single goal of image improvement.

Our previous publication (Biondi and Sava, 1999) established the theoretical framework of the method. We have presented the mathematical foundations of the method and a few simple experiments. Here we go one step further and present a complete example starting with the data at the surface and ending with an improved slowness model. Figure 2 shows a flowchart of our method, that consists of the following major loop:

1. Wave-equation migration,
2. image enhancement by residual migration in the angle domain,
3. velocity inversion,
4. slowness update and re-migration.

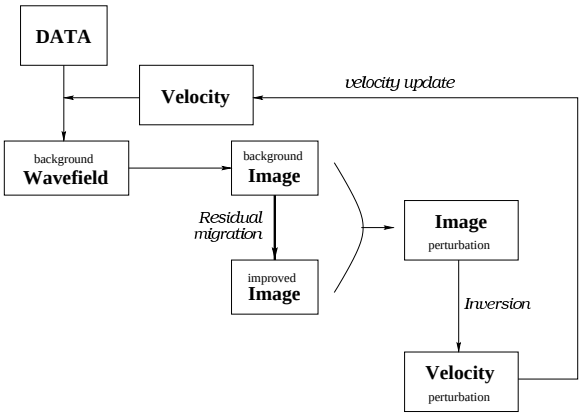

Figure 2: A flowchart of wave-equation migration and WEMVA. paul3-flow [NR]

Residual migration

Image enhancement is one of the most critical operations of the entire technique. Several methods can in theory be used to enhance the migrated image, for example, residual moveout and residual migration. The major difference between the two is that residual moveout does not allow energy to move among neighboring horizontal locations, while residual migration does. Sava (1999) shows how prestack Stolt residual migration can be employed to enhance migrated images described as angle-domain common-image gathers. In this paper, we use residual migration for image enhancement, but concentrate more on the results related to inversion and slowness update.

Slowness inversion

Once we have created an image perturbation , we can invert for the corresponding perturbation in slowness. Mathematically, this amounts to solving an optimization problem like (Claerbout, 1999)

$$\begin{aligned} \mathcal{L}\Delta\mathbf{s} &\approx \Delta\mathbf{R} \\ \epsilon\mathcal{A}\Delta\mathbf{s} &\approx 0, \end{aligned} \tag{1}$$

where

- $\mathcal{L}$ is a data-fitting operator, mainly composed of a scattering and a downward continuation operator, but which also incorporates the background wavefield (Biondi and Sava, 1999),
- $\mathcal{A}$ is a model-styling operator, either an isotropic Laplacian or an anisotropic steering-filter (Clapp and Biondi, 1998), which imposes smoothing on the model,
- $\Delta\mathbf{s}$ and $\Delta\mathbf{R}$ are respectively the slowness perturbation (the model) and the image perturbation (the data),
- ϵ is a scalar parameter controlling the weight of each of the individual goals.

To speed-up the inversion procedure, we can precondition the model in Equation 1 and solve the system

$$\begin{aligned} \mathcal{L}\mathcal{A}^{-1}\Delta\mathbf{p} &\approx \Delta\mathbf{R} \\ \epsilon\Delta\mathbf{p} &\approx 0, \end{aligned} \tag{2}$$

where $\Delta\mathbf{p} = \mathcal{A}\Delta\mathbf{s}$ is the preconditioned model variable.

Slowness update and the Born approximation

We generate the image perturbation by taking the difference between a reference image and an improved version of it. An underlying assumption of the inversion process is that we are within the Born approximation, which requires that the wavelets with which we operate are not more than $\pi/4$ out of phase. What happens if this condition is not fulfilled? In other words, what can we do if the enhanced image is so different from the original image that the wavelets we subtract are not in-phase anymore?

A possible answer to this question, although not necessarily the only one, is that we need to be conservative at the time we generate the improved image. For this, we can scale the velocity-ratio parameter surface (Sava, 1999), which controls the amount of enhancement in the image closer to unity, that is, closer to the original image (Figure 3).

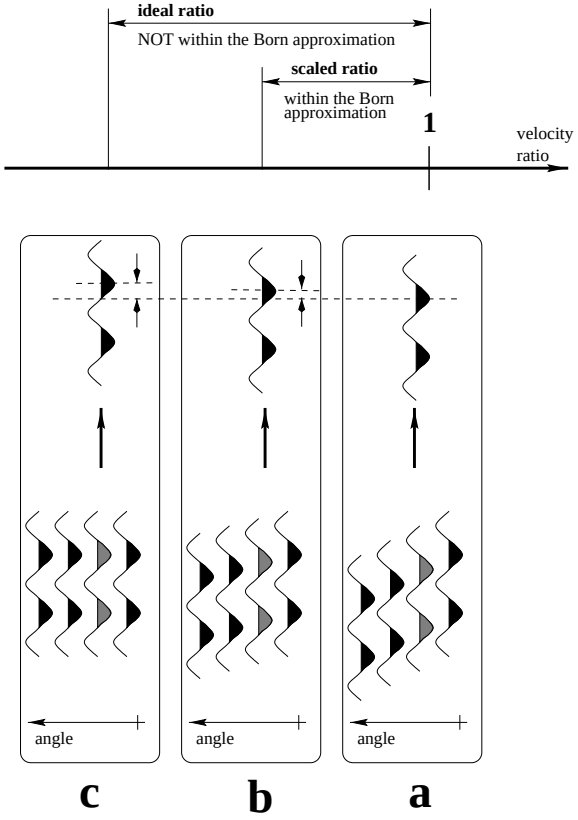

Figure 3: An illustration of velocity ratio scaling which makes the Born approximation valid. (a) is a gather extracted from the original image ($\gamma = 1$). (c) is the same gather after residual migration with the correct ratio. (b) is the same gather after residual migration with a scaled ratio. Although the ideal image is represented by (c), we cannot use this image because the wavelets are not within the Born approximation. Instead, we use (b), which is within the Born approximation and indicates the same direction of image improvement as the optimal ratio. paul3-ratscale [NR]

The shortcoming of this procedure is that we reduce the magnitude of image perturbation, although we preserve a more important parameter – its direction. The scaled-down restored image falls within the limits of the Born approximation with respect to the original; therefore, we can safely invert for the slowness perturbation. However, the slowness perturbation we obtain depends on the scaling we have done on the images, although it has the correct direction.

Next we need to scale the slowness perturbation back up to the value corresponding to the correct velocity ratio measured from the residual migrated images. So, how do we do this? A possible solution is to run a line search using the slowness perturbation we have inverted, with

the goal of maximizing the energy of the migrated image. Mathematically, this goal can be expressed as

$$\max_{\alpha} \| \mathcal{L}(\mathbf{s} + \alpha \Delta \mathbf{s}) \|, \tag{3}$$

where α is the scaling factor for the model, and $\mathbf{s}$ is the background slowness model.

EXAMPLE

We exemplify our velocity analysis technique using a synthetic model. The reflectivity, depicted in Figure 4, shows a structure with steeply dipping reflectors and an reverse fault. To complicate matters further, we set the slowness so that the fractured layer has higher velocity than the surrounding area (Figure 5). Although it doesn't seem difficult, this model is complicated by the severe distortion of the wavefield that propagates under the faulted region. Such a geological setting is common in overthrust regions and also around salt bodies.

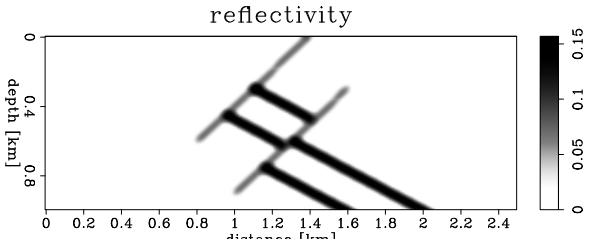

Figure 4: The reflectivity model. paul3-mod1.refl [CR]

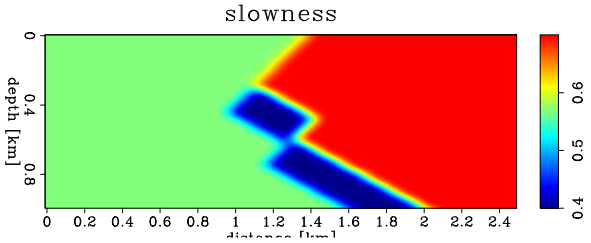

Figure 5: The true slowness model. paul3-mod1.Slow.0 [CR]

We begin by generating a synthetic dataset. Based on our simulated acquisition, defined by a half-offset of 2.0 km, we expect to achieve a reasonably good angular coverage of the region of interest, which is not deep.

The goal of this test is to start the imaging process by assuming that we don't know much about the slowness of the fast layer and to use our technique to fill the missing slowness. We run two separate tests: a simpler test when we assume that we know the geometry and slowness of the upper part of the model, and a more complex test when we do not assume anything about the slowness in the layer and attempt to fill it out entirely. [2]

[2]Throughout the rest of this paper, the figures corresponding to the first model have names with the prefix `mod1`, and the figures corresponding to the second model have names with the prefix `mod2`.

Model 1

As specified earlier, for model 1 we assume we do not have any information about the lower part of the fast velocity layer, but that we know the geometry and magnitude of the slowness in the upper segment. Figure 6 depicts the starting (background) slowness model. The background wavefield is significantly distorted by the strong slowness variation in the background, as shown in Figure 7.

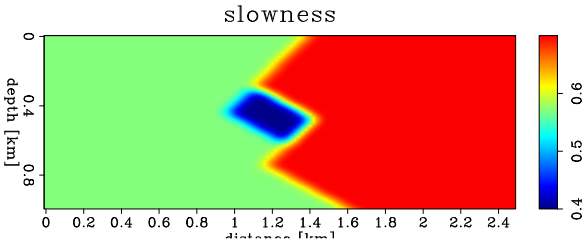

Figure 6: The starting slowness for model 1. This slowness model represents the background during the first pass (Figure 2). paul3-mod1.Slow.1 [CR]

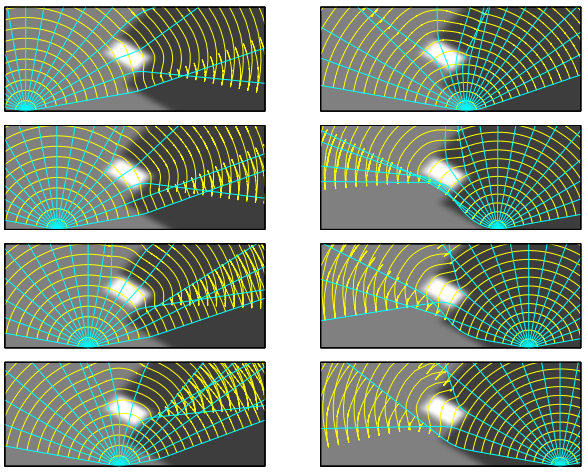

Figure 7: Rays and wavefronts for different source points in the subsurface. The wavefield triplicates because of the strong slowness variation in the background. paul3-mod1.rays [CR]

Next, we migrate the synthetic data using the background slowness. The resulting image (Figure 8) is perfect in the upper part of the section, above the area with inaccurate slowness, but it is not completely accurate in the lower part, where the incorrect slowness model limits our imaging abilities. To analyze the quality of the image, we display it as angle-domain common image gathers (Prucha et al., 1999; Sava and Fomel, 2000) that have the property of showing flat events when the migration velocity is correct, and bending events when the velocity is incorrect.

In the next step, we compute an improved image (Figure 9) following the methodology outlined earlier in this paper and fully described in (Sava, 1999). As expected, there is no improvement in the upper section, since the velocity model is correct there, but only in the lower section, under the fault region. The picked velocity ratio surface is presented in Figure 10.

Finally, we can take the background (Figure 8) and enhanced (Figure 9) images and compute the image perturbation, depicted in Figure 11. For comparison, Figure 12 shows the theoretically-correct image perturbation computed using the true slowness to migrate the data.

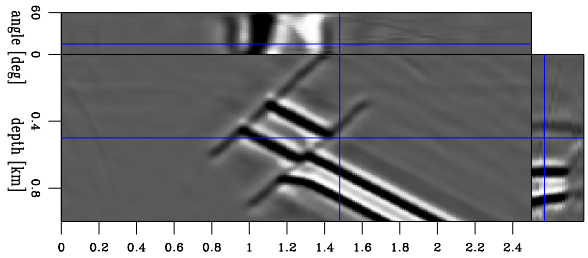

Figure 8: The background image for model 1 presented as angle-domain common image gathers. The correctly migrated events are flat, while those incorrectly migrated are not, for example at the bottom of the lower layer. paul3-mod1.bimg.1 [CR]

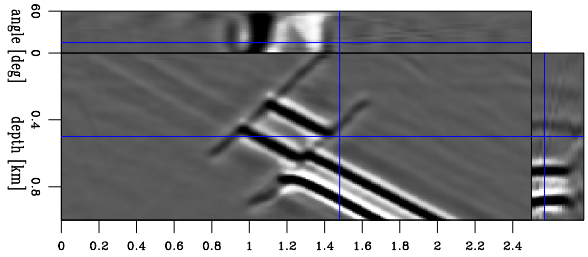

Figure 9: The enhanced image for model 1. paul3-mod1.aimg.1 [CR]

Although the two images are not identical, they are similar. In practice, our goal is to come as close as possible to the image in Figure 12.

We have reached the point where we have created an image perturbation. We can now go one step further and compute the perturbation in slowness by solving the least-squares systems in Equations (1) or (2).

Figure 13 shows the result of the inversion process without any model regularization [$\epsilon = 0$ in equation (2)]. Every panel in the figure represents one iteration, as indicated by its title. The anomaly we seek is nicely recovered, with its position confined to the right area, as indicated by the schematic overlay. The absolute magnitude of the anomaly is smaller than that of the true one. This result can probably be explained by the nature of the Born approximation and the scaling of the velocity ratio surface. The definitive answer, however, is subject to further research.

Even though we have not yet imposed any smoothness constraint on the model, the anomaly is reasonably smooth, which is a direct consequence of the band-limited character of our wave-equation processing. The image is also free of major artifacts, although the bottom area of the model, which is not constrained by anything in the image perturbation, develops an anomaly of the opposite sign and another small, blob-like anomaly, possibly a wrap-around artifact.

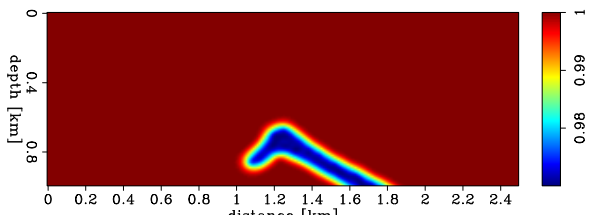

Figure 10: The picked velocity ratio surface for model 1. This surface has values different from 1 only in the areas where the image has changed as a result of residual migration. paul3-mod1.lmap.1 [CR]

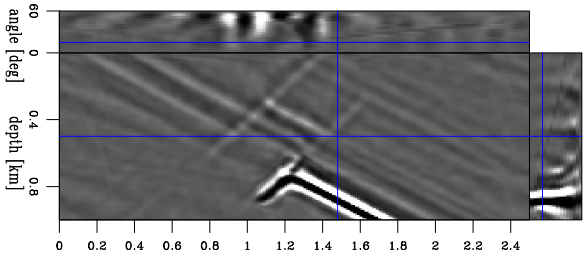

Figure 11: The image perturbation for model 1 computed from the background image and the image enhanced by residual migration. paul3-mod1.dimg.1 [CR]

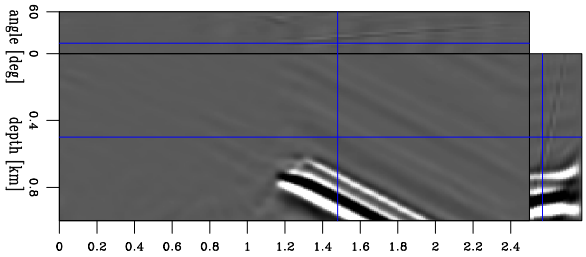

Figure 12: The perturbation in image for model 1 computed from the background image and the image obtained through migration with the true slowness. paul3-mod1.dimg.0 [CR]

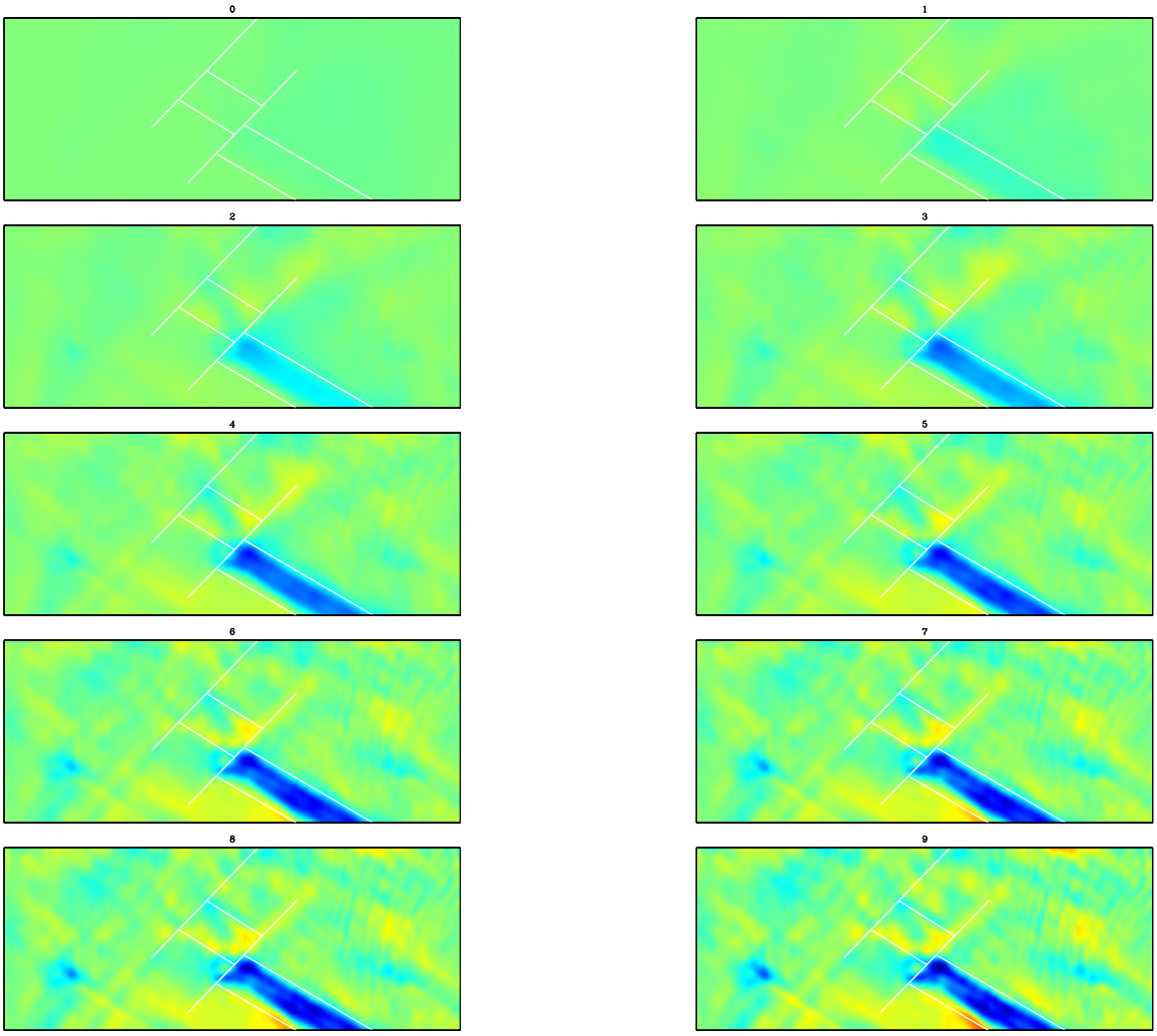

Figure 13: Iteration panels for the unregularized inversion in the case of model 1. paul3-mod1.inv.plain.1 [CR]

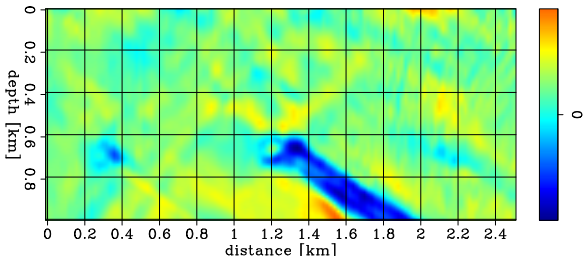

Figure 14: Unregularized solution for model 1 after the first loop. paul3-mod1.sol.plain.1 [CR]

Figure 15 shows the result of model inversion for the regularized system (Equations 1). The anomaly is even smoother and confined to its correct location. Figures 14 and 16 show the final inversion result for the unregularized case and the case of preconditioning the model with a steering filter that forces the data to spread more along the geological dip and less perpendicular to it.

Finally, we update the background slowness model and repeat the loop. Figure 17 shows the updated background slowness, and Figure 18 the new background image. This new image should be compared to the previous background image (Figure 8). Notably, the bottom layer is pushed in depth closer to its correct position, and the angle-domain common image gathers show, on the average, flatter events, indicating that the new image is migrated with better velocity. The slowness perturbation is scaled differently before summation, as guided by the line-search optimization (Equation 3). We repeat the loop and obtain the slowness perturbation shown in Figure 19 and the updateded image shown in Figure 20.

Here are the main conclusions we can derive from the first example:

- The image perturbation produced with residual migration is reasonably good, even for the case of a model with significant wavefield distortions in the background.
- As expected, wave-equation inversion produces smooth results, because of the intrinsic band-limited nature of wave propagation. Model regularization, however, helps to produce an even smoother slowness perturbation.
- The magnitude of the slowness anomaly we produced after inversion is less than the correct one. This is, in part, explained by the various approximations made when we created the image perturbation. It remains, nevertheless, an interesting topic that requires further investigation.
- The updated background slowness is able to produce an improved image, measured by the flatness of the angle-domain common image gathers. In other words, we have fulfilled the main goal of our procedure – image improvement– at the same time that we have improved the slowness model.
- Two WEMVA loops do not seem to be enough to recover the full slowness perturbation. We can get better results if we loop more, although cost remains a significant limitation. Here we have another direction of future work.

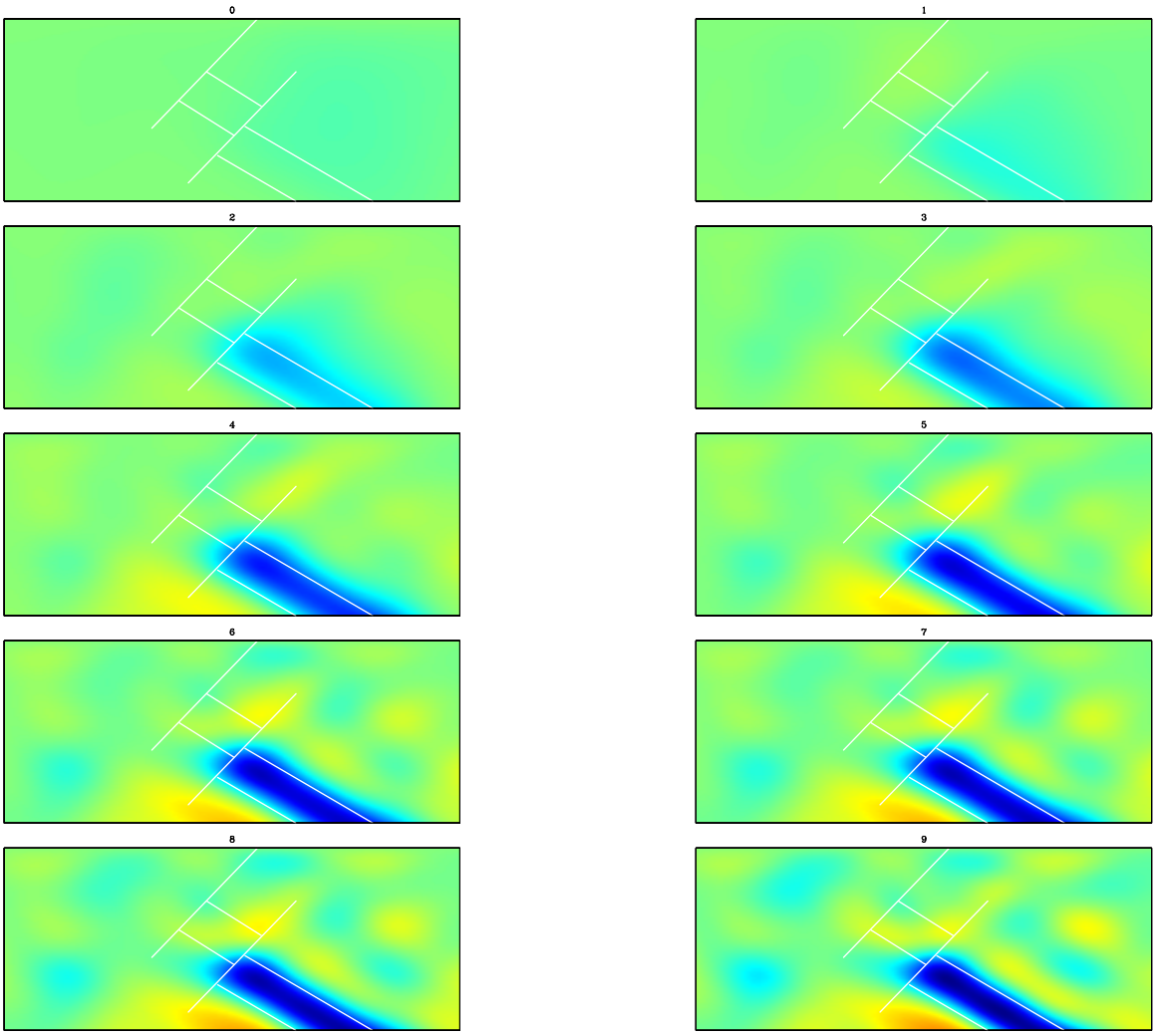

Figure 15: Iteration panels for the preconditioned inversion in the case of model 1. paul3-mod1.inv.laplacian.1 [CR]

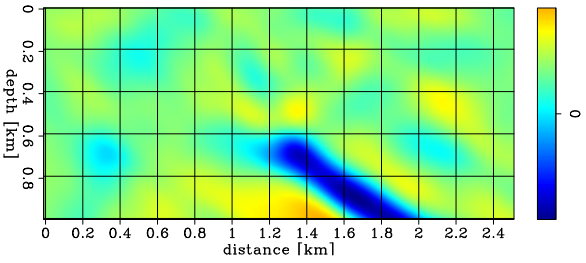

Figure 16: Solution for model 1 after the first loop in the case of regularization with steering filters. paul3-mod1.sol.steering.1 [CR]

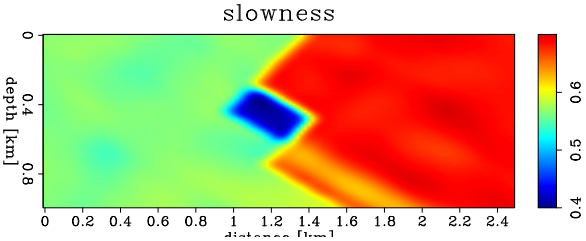

Figure 17: Updated background slowness for model 1 after the first loop. paul3-mod1.Slow.2 [CR]

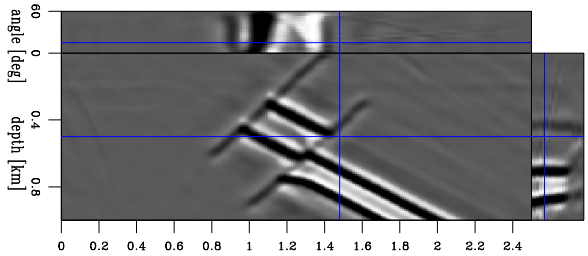

Figure 18: The updated background image for model 1 after the first loop. paul3-mod1.bimg.2 [CR]

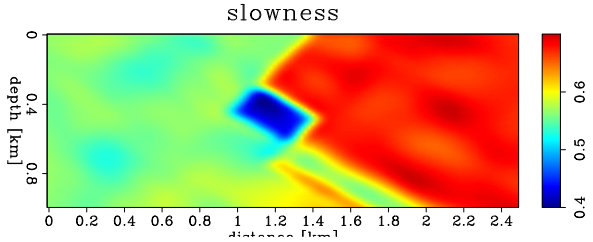

Figure 19: Updated background slowness for model 1 after the second loop. The line search procedure gives the slowness perturbation scaling parameter $\alpha = 0.625977$. paul3-mod1.Slow.3 [CR]

Model 2

The second model we use to illustrate our procedure is derived from the same synthetic structure. This model differs from the first in that we now assume that we have no information about both the lower and the upper parts of the layer. The aim of this model is to recover the slowness anomaly, both in the upper and the lower sections.

For this second model, we follow the same basic steps as for the previous model. Here are the results:

1. Figure 21 represents the background slowness model. The fast layer is missing completely in this example.

2. Figure 22 represents rays and wavefronts for different shooting locations in the subsurface. The background wavefield is distorted, but not as much as in the case of the first model. This would indicate that this example is easier than the first one, although it probably doesn't make a significant difference because WEMVA handles naturally complex wavefields.

3. Figure 23 is the background image for model 2. Correctly migrated events are flat, while the incorrect ones are not. The background image is similar to the one in the

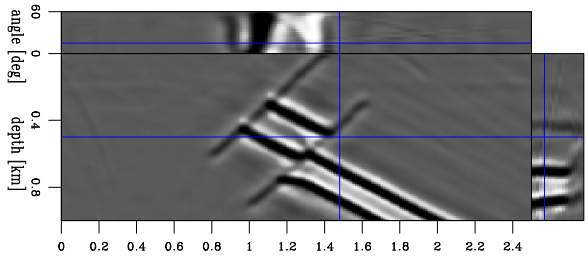

Figure 20: The updated background image for model 1 after the second loop. The line search procedure gives the slowness perturbation scaling parameter $\alpha = 1.0262$. paul3-mod1.bimg.3 [CR]

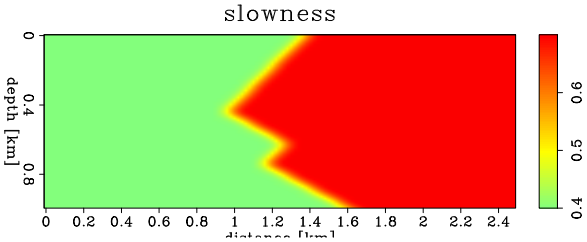

Figure 21: The starting slowness for model 2. It represents the background during the first pass (Figure 2). paul3-mod2.Slow.1 [CR]

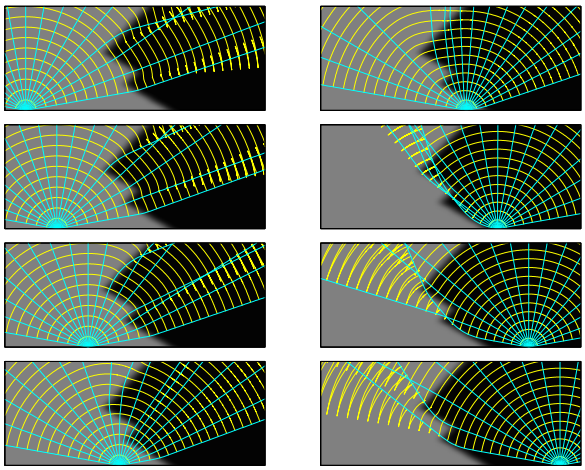

Figure 22: Rays and wavefronts for different source points in the subsurface. The wavefield for model 2 also triplicates because of the slowness variation in the background, but not as strongly as in the case of the first model. paul3-mod2.rays [CR]

preceding example (Figure 8), but it is distorted more, especially in the upper segment of the faulted layer.

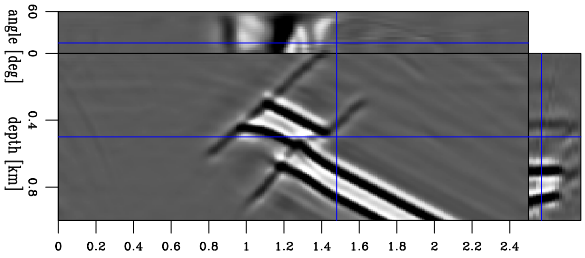

Figure 23: The background image for model 2 presented as angle-domain common image gathers. Correctly migrated events are flat, while the incorrect ones are not. paul3-mod2.bimg.1 [CR]

4. Figure 24 is the image enhanced by residual migration. Figure 25 is the corresponding picked velocity ratio surface.

5. Figure 26 is the image perturbation computed from the background image (Figure 23) and the image enhanced by residual migration (Figure 24). For comparison, Figure 27 is the image perturbation obtained through the difference of the images migrated with the true and background slowness functions.

6. Figure 28 are the iteration panels for unregularized inversion, and Figure 29 are the iteration panels for preconditioned inversion. Here we can see the major differences and similarities between this and the first example: the lower part of the layer is well recovered; the upper part of the layer is also recovered reasonably well, although not as well as the lower part. The region around the fault, however, is not constrained enough

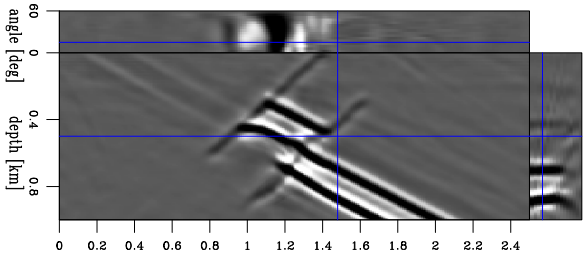

Figure 24: The enhanced image for model 2. paul3-mod2.aimg.1 [CR]

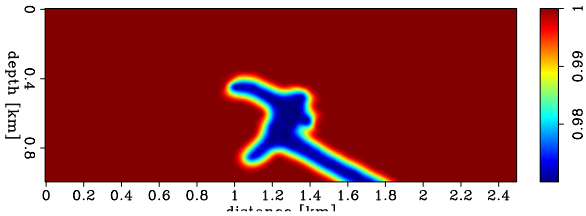

Figure 25: The picked velocity ratio surface for model 2. paul3-mod2.lmap.1 [CR]

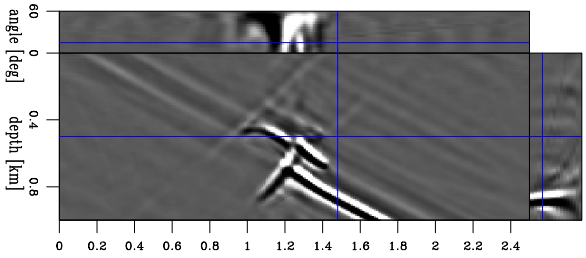

Figure 26: The image perturbation for model 2 computed from the background image and the image enhanced by residual migration. paul3-mod2.dimg.1 [CR]

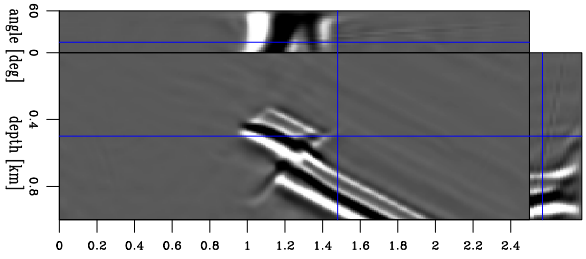

Figure 27: The image perturbation for model 2 computed from the background image and the image obtained through migration with the true slowness. paul3-mod2.dimg.0 [CR]

and shows high spatial-frequency variation in slowness (Figure 28). However, if we regularize the model during the inversion, we recover a much smoother anomaly. The most significant change occurs in the area surrounding the fault. In this case, we do not observe the large fluctuations that occur in the unregularized example, although the regularization operator causes the slowness anomaly to leak outside its bounds.

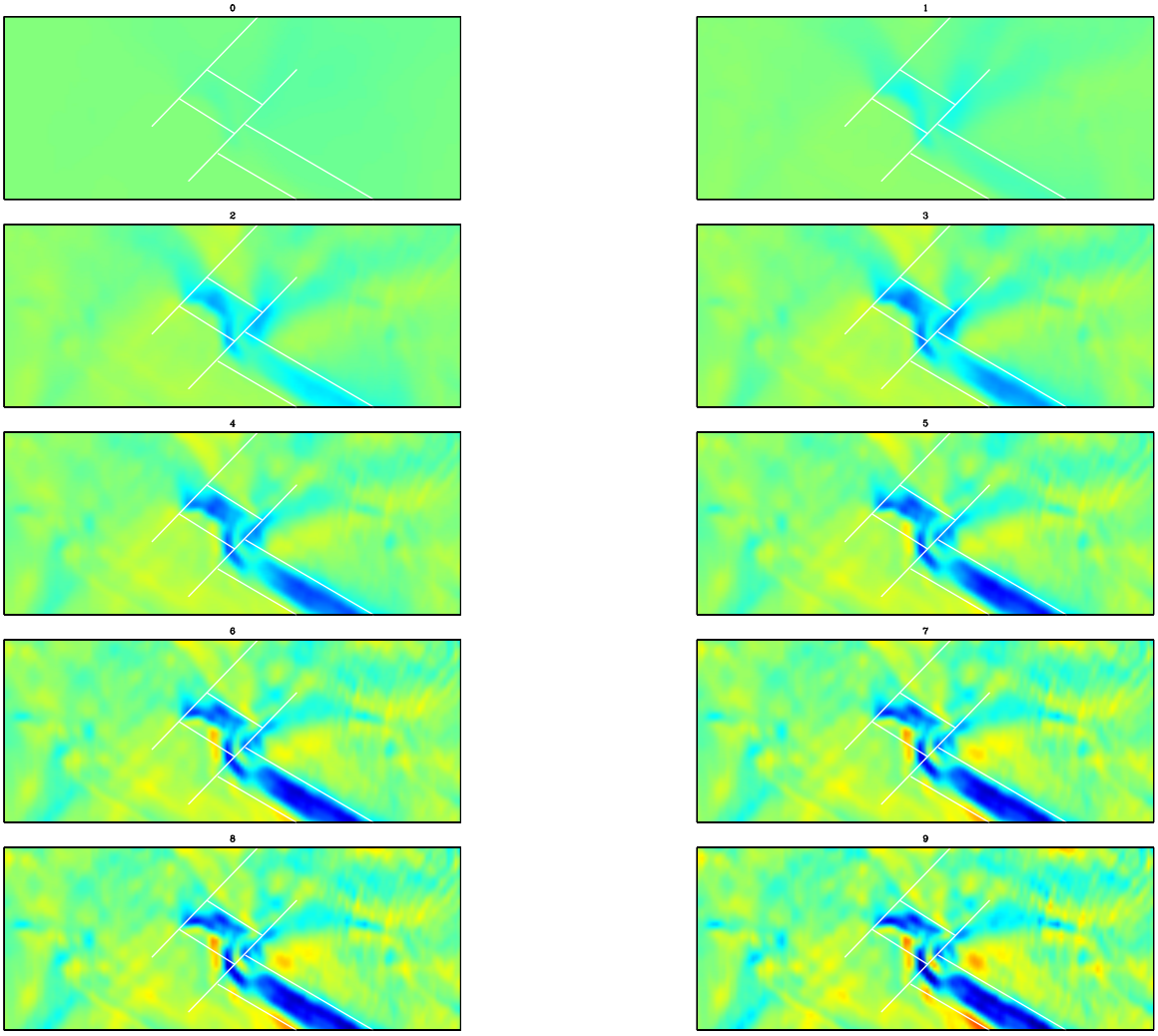

Figure 28: Iteration panels for the unregularized inversion in the case of model 2. paul3-mod2.inv.plain.1 [CR,M]

7. Figure 30 is the unregularized solution after the first loop, and Figure 31 is the solution after the first loop when the model is regularized using steering filters. The second of the two is a significantly improved result: the anomaly is much smoother, and the leakage in the vertical direction outside the layer bounds is reduced compared to the case of preconditioning with an isotropic Laplacian operator.

8. Figure 32 is the updated background slowness after the first loop, and Figure 33 is the corresponding updated background image. Although not yet completely there, the fast

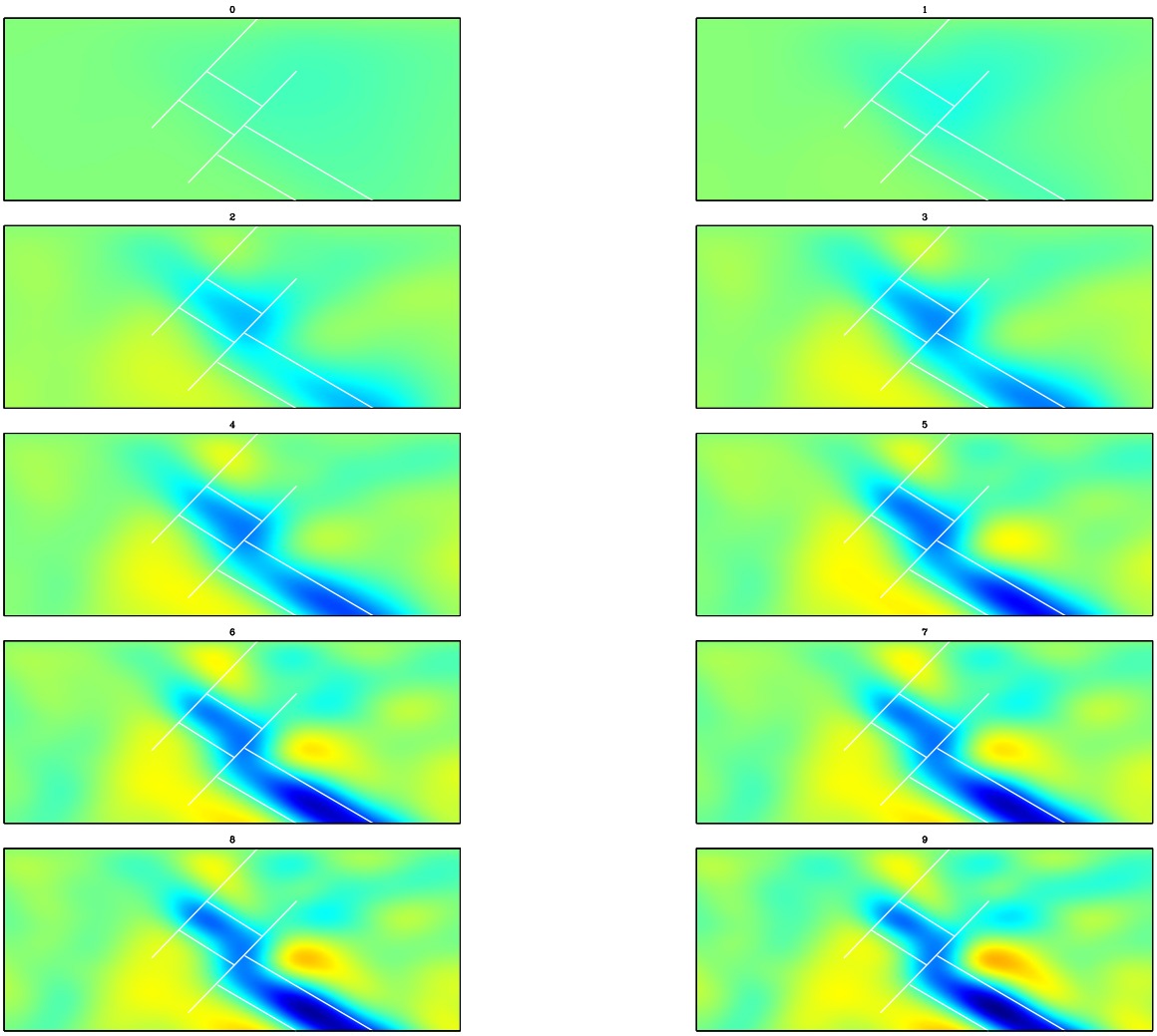

Figure 29: Iteration panels for the preconditioned inversion in the case of model 2. paul3-mod2.inv.laplacian.1 [CR,M]

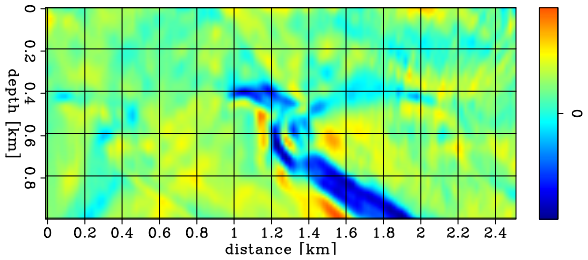

Figure 30: Unregularized solution for model 2 after the first loop. paul3-mod2.sol.plain.1 [CR]

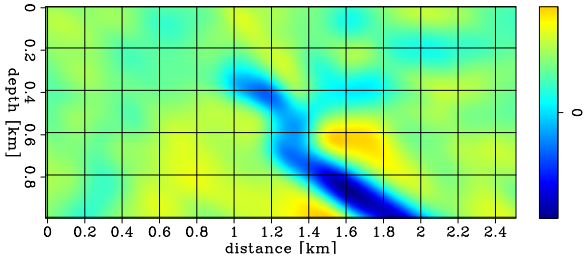

Figure 31: Solution for model 2 after the first loop in the case of regularization with steering filters. paul3-mod2.sol.steering.1 [CR]

layer begins to build-up, and, consequently, the quality of the migrated image improves. However, we have not reached a satisfactory image at every location; therefore, we need to repeat the WEMVA loop. When we repeat the loop we obtain the slowness perturbation shown in Figure 34 and the updateded image shown in Figure 35.

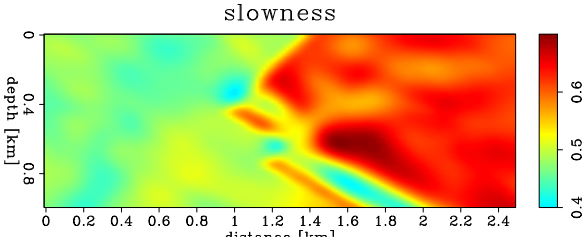

Figure 32: Updated background slowness for model 2 after the first loop. The line search procedure gives the slowness perturbation scaling parameter $\alpha = 1.64043$. paul3-mod2.Slow.2 [CR]

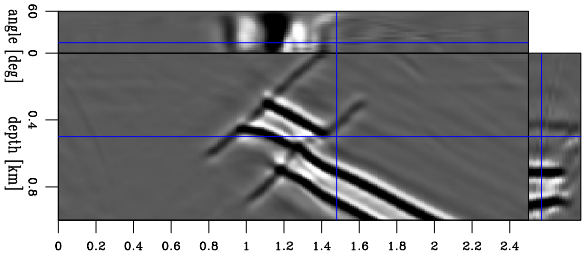

Figure 33: The updated background image for model 2 after the first loop. paul3-mod2.bimg.2 [CR]

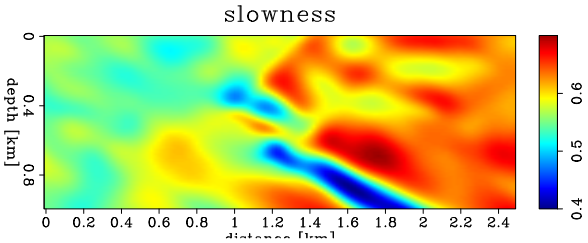

Figure 34: Updated background slowness for model 2 after the second loop. The line search procedure gives the slowness perturbation scaling parameter $\alpha = 2.81967$. paul3-mod2.Slow.3 [CR]

The main conclusions we can derive from the second example are:

- Residual migration is successful in producing a good image perturbation, even though the starting image is more complex and significantly more distorted than in the first case.
- The anomaly produced by WEMVA without model regularization does not have as high a quality as it does in the original case. Large distortions in the original image, possibly coupled with residual migration distortions, lead to high spatial frequency variations of the inverted anomaly. We can, however, control the shape of the anomaly with smoothness constraints on the model, among which steering filters produce a promising result.
- The updated image is characterized by flatter angle-domain common image gathers. One loop, however, doesn't seem to be enough to achieve a completely satisfactory result, and we need to iterate more.

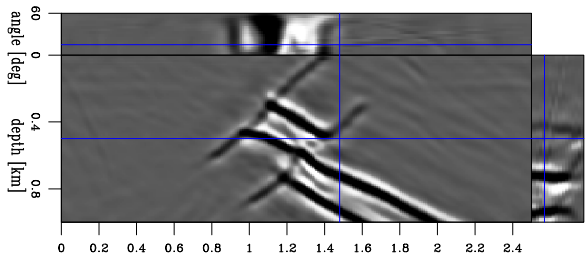

Figure 35: The updated background image for model 2 after the second loop. paul3-mod2.bimg.3 [CR]

CONCLUSIONS

In this paper, we demonstrated the feasibility of migration velocity analysis using wave-equation methods. The results we obtained on 2-D synthetic models are very encouraging. Cost remains a major limitation, although as our method progressively matures, we have more and more computer power at our disposal.

The main point we would like to make is that unlike other velocity inversion techniques, our method updates the velocity model by improving the quality of the migrated image, and not by fitting the recorded data. It therefore takes full advantage of the intertwined nature of migration and velocity analysis,

Wave-equation migration techniques are known for their potential to handle complex wavefields. Since our velocity analysis method is also based on processing with the wave-equation, it inherits stability and constrains the derived velocity to be smoother than what a traveltime-based method would allow. Furthermore, we can control the shape of our derived velocity anomalies by imposing external constraints, either model-independent, like Laplacian smoothing, or model-dependent steering filters.

The Born approximation on which we base our method limits the amount of improvement we can allow on the starting image. For lack of a better procedure, we now chose to continue with a technique in which we scale-down the image perturbation and later scale-up the slowness perturbation. Handling the limitations imposed by the Born approximation is one of the most useful and exciting areas of future research.

In addition to improvements in scaling and rescaling the image and slowness perturbations, other potential directions of future research include semblance and differential semblance analysis for more reliable image enhancements and an analysis of the implications of the complex nature of the wavefields, specifically the benefits of implicitly using all the arrivals in the wavefield for velocity analysis rather than merely a single one.

REFERENCES

Biondi, B., and Sava, P., 1999, Wave-equation migration velocity analysis: SEP–**100**, 11–34.

Claerbout, J., 1999, Geophysical estimation by example: Environmental soundings image enhancement: http://sepwww.stanford.edu/sep/prof/.

Clapp, R. G., and Biondi, B. L., 1998, Regularizing time tomography with steering filters: SEP–**97**, 137–146.

Gray, S. H., 1998, Speed and accuracy of seismic migration methods: Mathematical Geophysical Summer School, Stanford University.

Prucha, M. L., Biondi, B. L., and Symes, W. W., 1999, Angle-domain common image gathers by wave-equation migration: SEP–**100**, 101–112.

Sava, P., and Fomel, S., 2000, Angle-gathers by Fourier Transform: SEP–**103**, 119–130.

Sava, P., 1999, Enhancing common-image gathers with prestack Stolt residual migration: SEP–**102**, 47–60.

APPENDIX

This appendix is a picture summary of the processing we describe in the paper. We present four figures for each of the two models we discuss in the earlier sections.

- Figures (A-1,A-2) and (A-5,A-6) describe the first two WEMVA loops (Figure 2) for models 1 and 2, respectively. From top to bottom, the panels depict
  - the background slowness model,
  - the background image,
  - the image improved by residual migration, and
  - the perturbation in image derived from the background and improved images.
- Figures A-3 and A-7 describe the changes on the slowness model for the first two WEMVA loops (Figure 2). From top to bottom, the panels depict
  - the correct slowness,
  - the background slowness,
  - the updated slowness after the first loop, and
  - the updated slowness after the second loop.
- Figures A-4 and A-8 describe the changes that are induced on the image for the first two WEMVA loops (Figure 2). From top to bottom, the panels depict
  - the image migrated with the true slowness,
  - the image migrated with the starting slowness,
  - the image migrated with the slowness updated after the first loop, and
  - the image migrated with the slowness updated after the second loop.

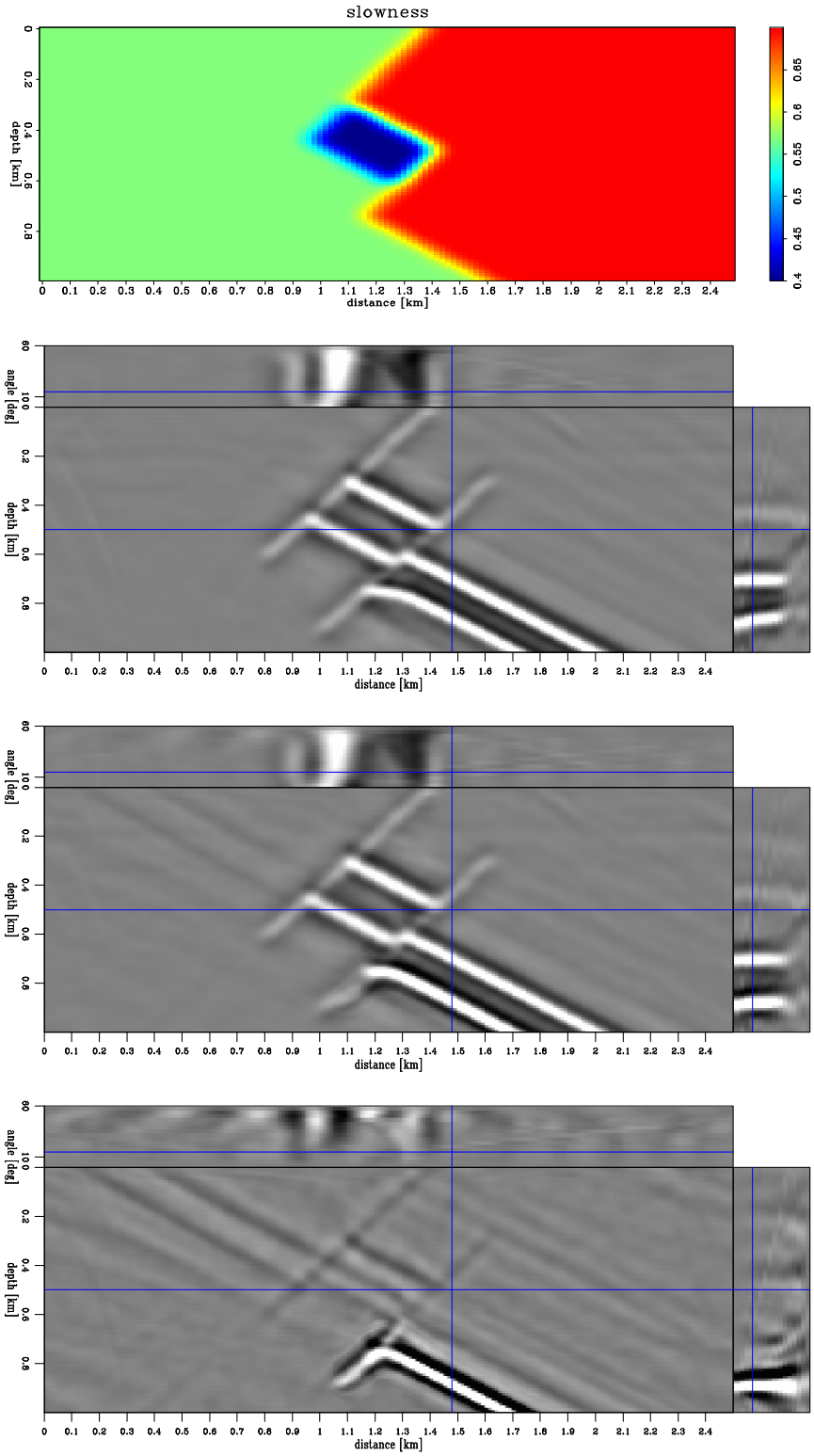

Figure A-1: Model 1, WEMVA loop 1. From top to bottom: background slowness, background image, improved image, and image perturbation. paul3-mod1.loop.1 [CR]

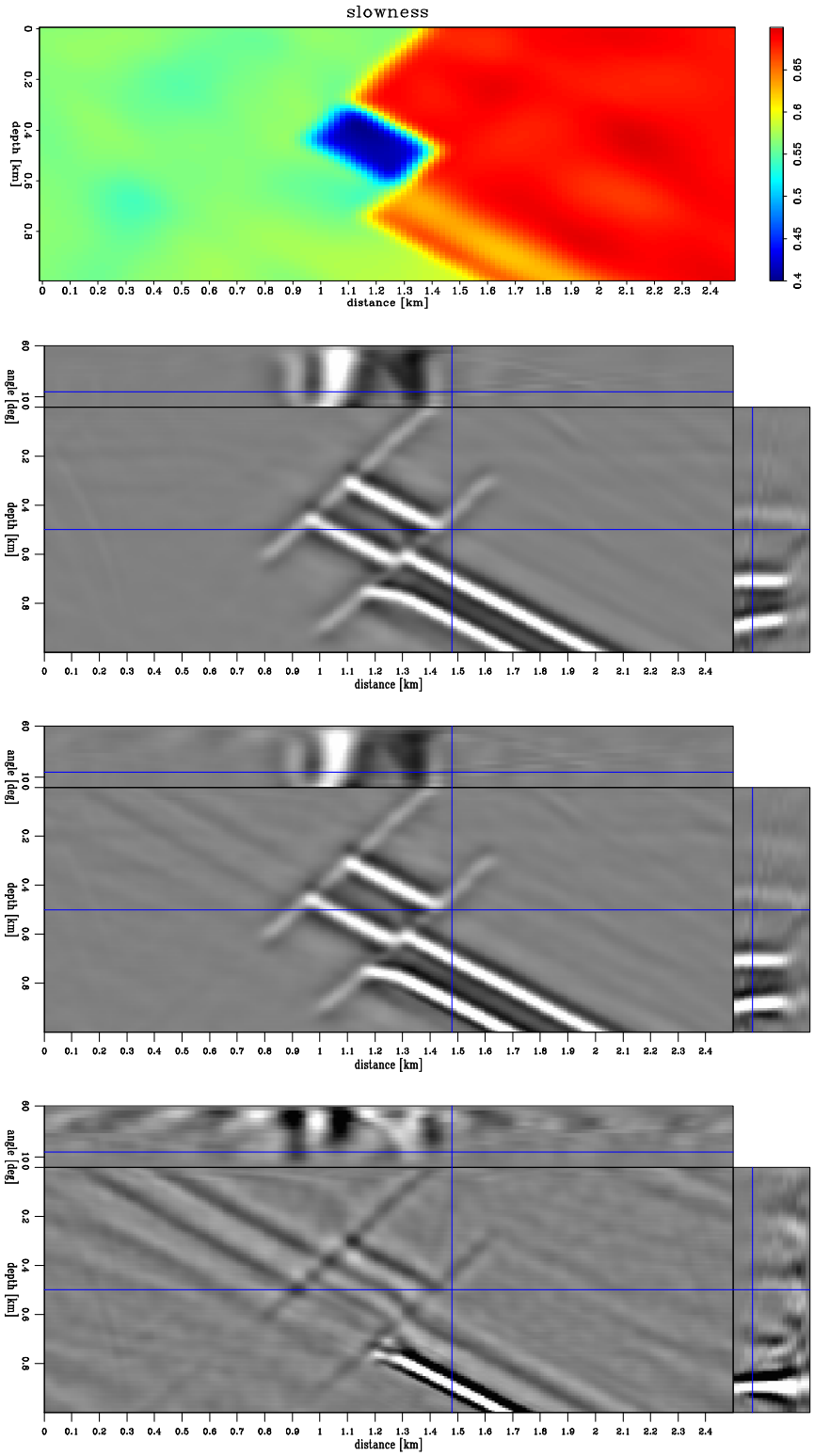

Figure A-2: Model 1, WEMVA loop 2. From top to bottom: background slowness, background image, improved image, and image perturbation. paul3-mod1.loop.2 [CR]

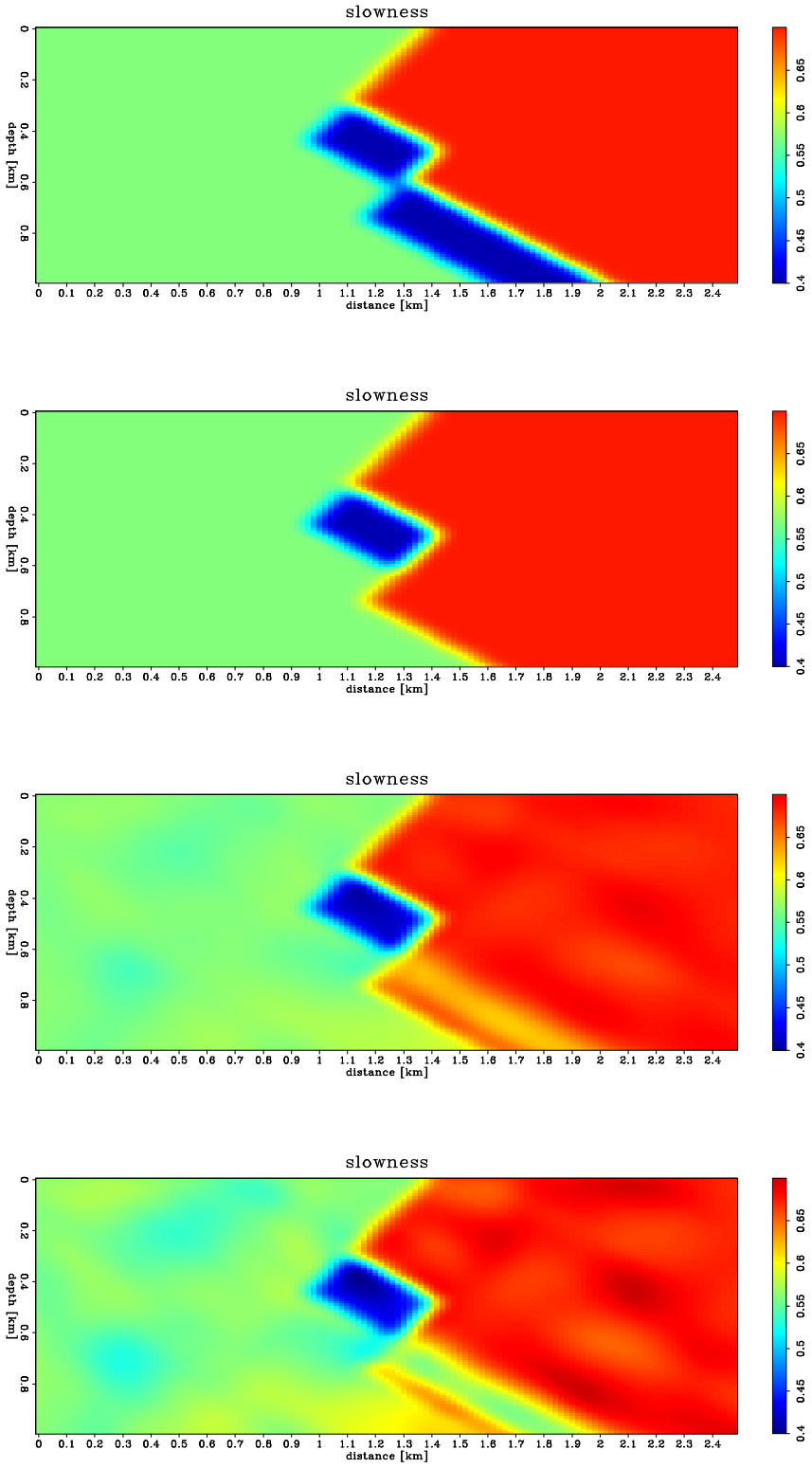

Figure A-3: Model 1, summary of slowness changes with loop number. From top to bottom: the true slowness, the starting slowness, the slowness updated after the first loop, the slowness updated after the second loop. paul3-mod1.slows [CR]

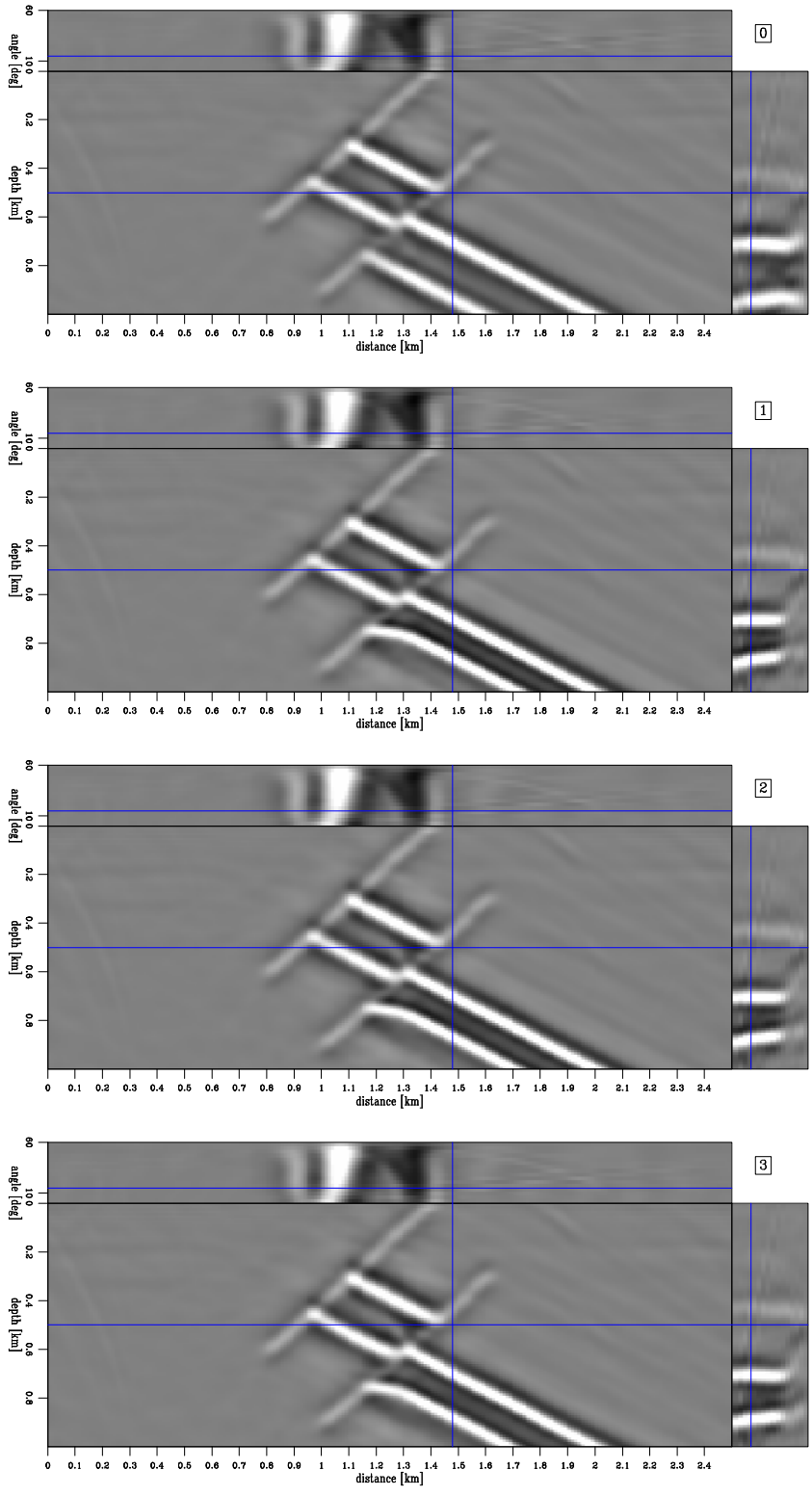

Figure A-4: Model 1, summary of image changes with loop number. From top to bottom, images obtained with the true slowness, the starting slowness, the slowness updated after the first loop, the slowness updated after the second loop. paul3-mod1.iter [CR]

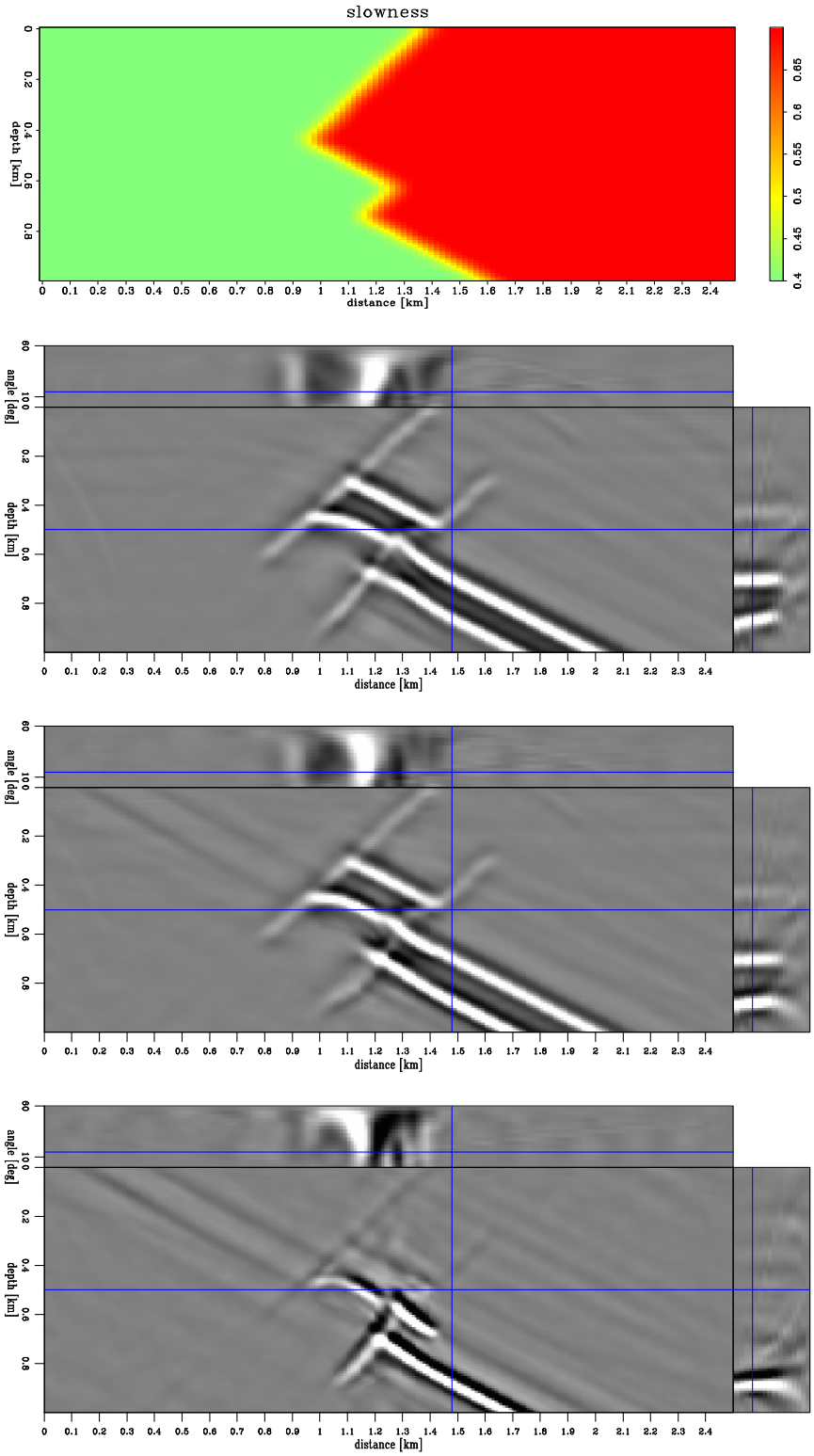

Figure A-5: Model 2, WEMVA loop 1. From top to bottom: background slowness, background image, improved image, and image perturbation. paul3-mod2.loop.1 [CR]

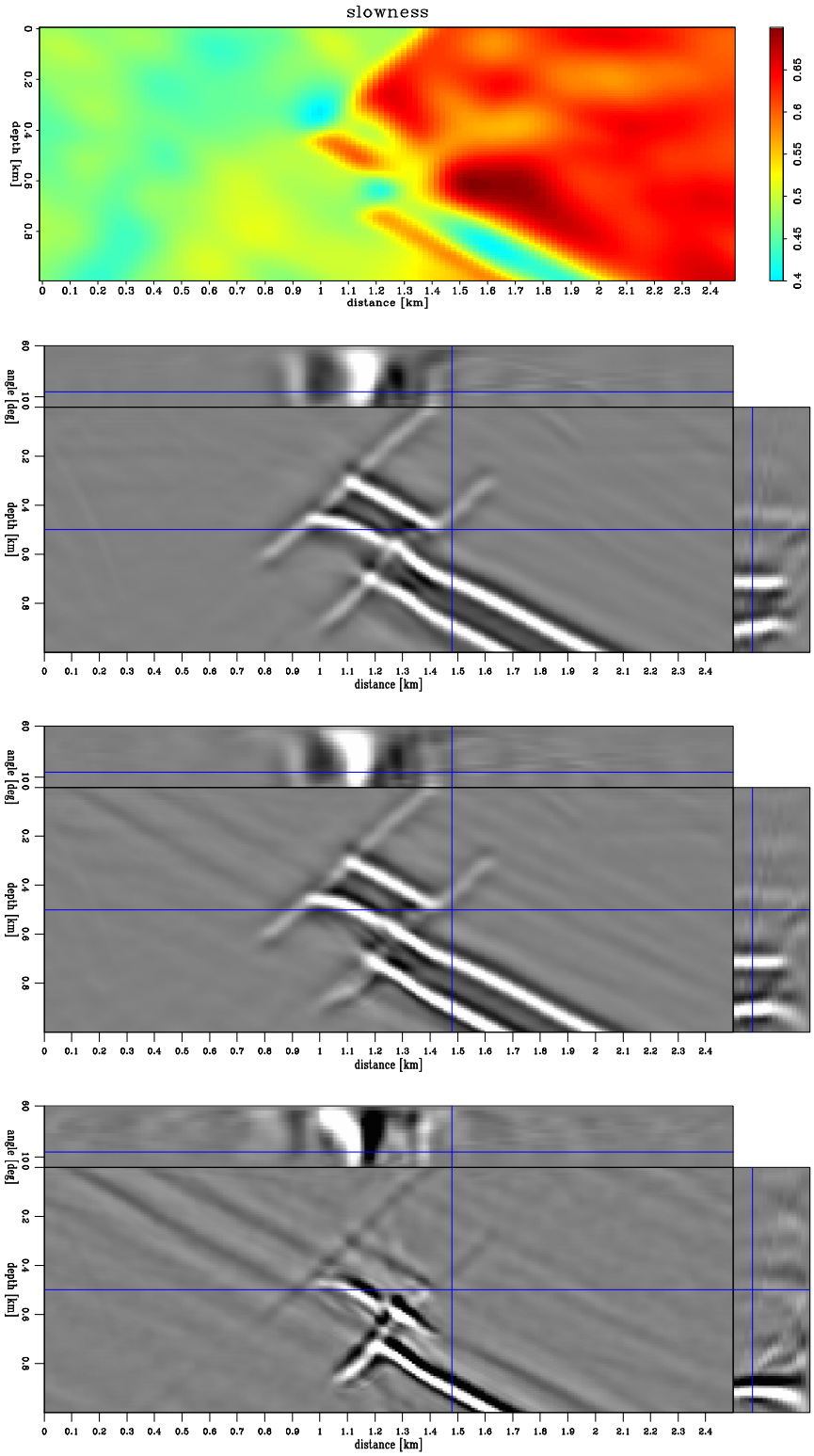

Figure A-6: Model 2, WEMVA loop 2. From top to bottom: background slowness, background image, improved image, and image perturbation. paul3-mod2.loop.2 [CR]

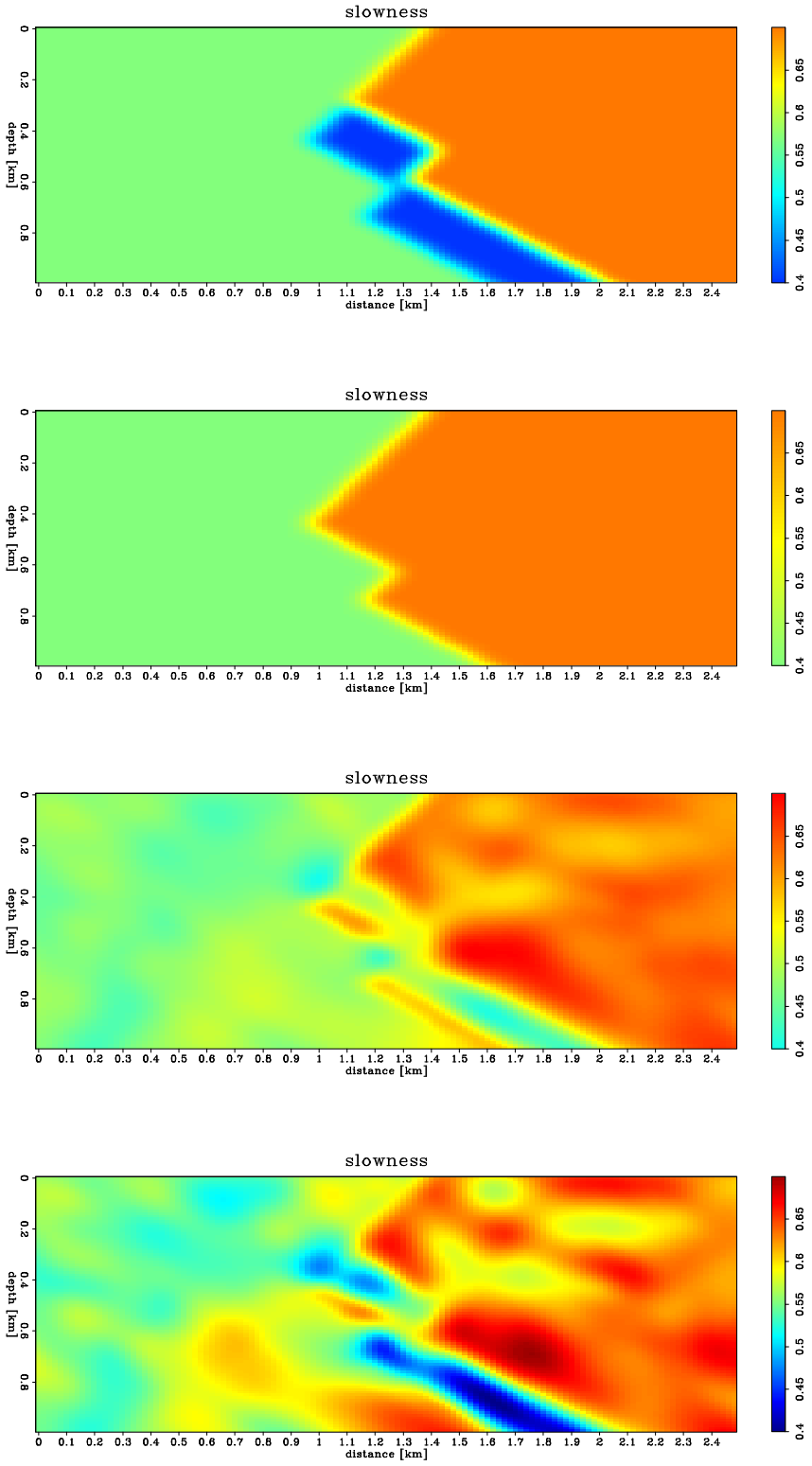

Figure A-7: Model 2, summary of slowness changes with loop number. From top to bottom: the true slowness, the starting slowness, the slowness updated after the first loop, the slowness updated after the second loop. paul3-mod2.slows [CR]

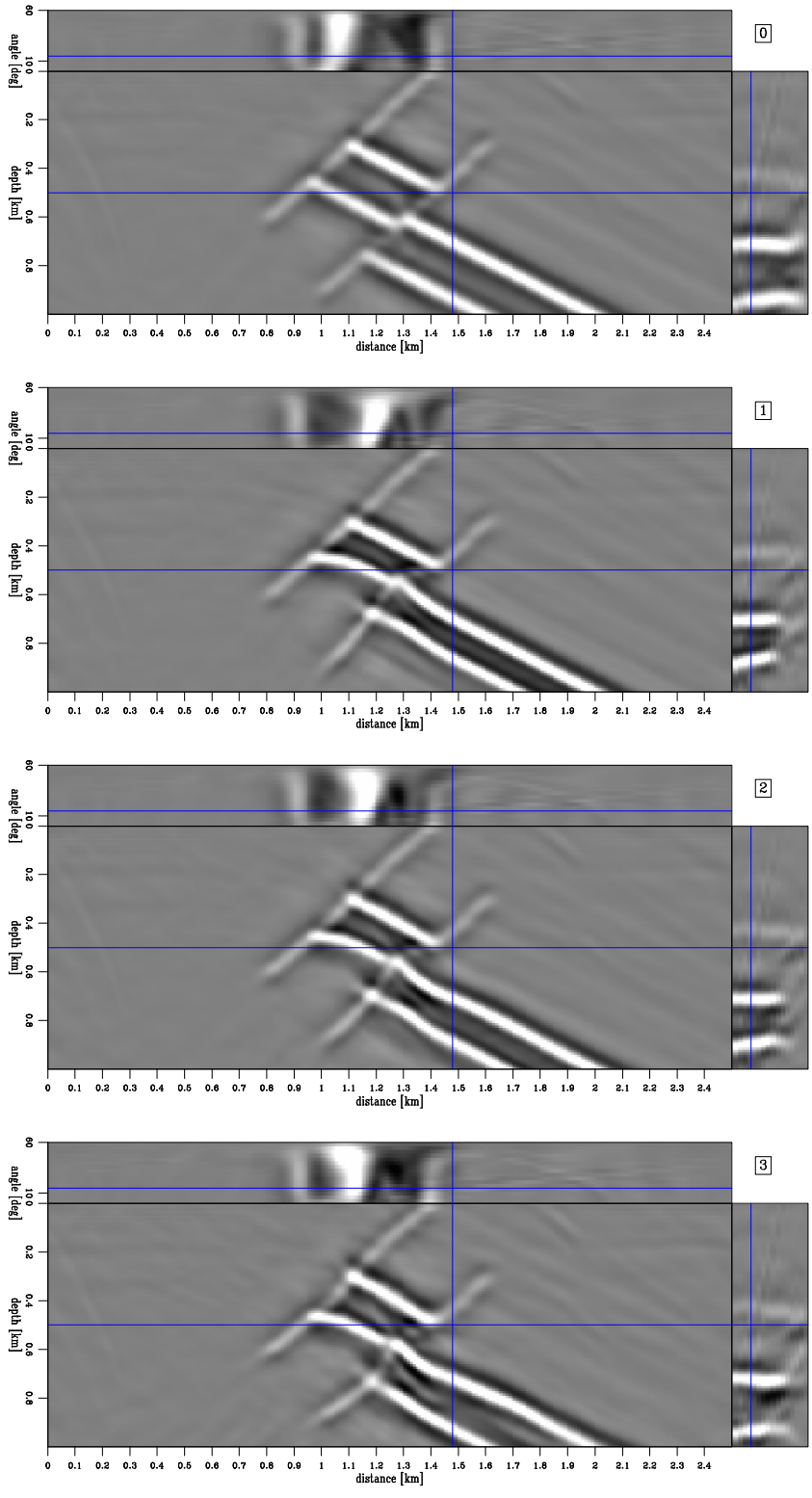

Figure A-8: Model 2, summary of image changes with loop number. From top to bottom, images obtained with the true slowness, the starting slowness, the slowness updated after the first loop, the slowness updated after the second loop. paul3-mod2.iter [CR,M]